Published in final edited form as:
Bone. 2011 March 1; 48(3): 578–587. doi:10.1016/j.bone.2010.11.003.

Combined Inhibition of the BMP pathway and the RANK-RANKL axis in a Mixed Lytic/blastic Prostate Cancer Lesion

Mandeep S. Virk[1], **Farhang Alaee**[1], **Frank A. Petrigliano**[2], **Osamu Sugiyama**[1], **Arion F. Chatziioannou**[3], **David Stout**[3], **William C. Dougall**[4], and **Jay R. Lieberman**[1,†]

[1] New England Musculoskeletal Institute, Department of Orthopaedic Surgery, University of Connecticut Health Center, 263 Farmington Avenue, Farmington, CT 06030-5456, USA

[2] Department of Orthopaedic Surgery, David Geffen School of Medicine, University of California at Los Angeles, Center for Health Sciences 76-134, 10833 LeConte Avenue, Los Angeles, CA 90095, USA

[3] The Crump Institute for Molecular Imaging, Department of Molecular and Medical Pharmacology, University of California at Los Angeles, 700 Westwood Boulevard, Los Angeles, CA 90095, USA

[4] Department of Hematology and Oncology Research, 1201 Amgen Court West, Seattle, WA 98119-3105

Abstract

The purpose of this study was to investigate the influence of combined inhibition of RANKL (receptor activator of nuclear factor kappa-B ligand) and bone morphogenetic protein (BMP) activity in a mixed lytic/blastic prostate cancer lesion in bone. Human prostate cancer cells (C4 2b) were injected into immunocompromised mice using an intratibial injection model to create mixed lytic/blastic lesions. RANK-Fc, a recombinant RANKL antagonist, was injected subcutaneously three times a week (10mg/kg) to inhibit RANKL and subsequent formation, function and survival of osteoclasts. Inhibition of BMP activity was achieved by transducing prostate cancer cells *ex vivo* with a retroviral vector expressing noggin (retronoggin; RN). There were three treatment groups (RANK-Fc treatment, RN treatment and combined RN and RANK-Fc treatment) and two control groups (untreated control and empty vector control for the RN treatment group). The progression of bone lesion and tumor growth was evaluated using plain radiographs, hind limb tumor size, ^{18}F-Fluorodeoxyglucose and ^{18}F-fluoride micro PET-CT, histology and histomorphometry. Treatment with RANK-Fc alone inhibited osteolysis and transformed a mixed lytic/blastic lesion into an osteoblastic phenotype. Treatment with RN alone inhibited the osteoblastic component in a mixed lytic/blastic lesion and resulted in formation of smaller osteolytic bone lesion with smaller soft tissue size. The animals treated with both RN and RANK-Fc demonstrated delayed development of bone lesions, inhibition of osteolysis, small soft tissue tumors and preservation of bone architecture with less tumor induced new bone formation. This study suggests that combined inhibition of the RANKL and the BMP pathway may be an

Corresponding author's address: Jay R. Lieberman, M.D., The New England Musculoskeletal Institute, Department of Orthopaedic Surgery, University of Connecticut Health Center, 263 Farmington Avenue, Farmington, Connecticut 06030-5456, Tel: 860-679-2640; Fax: 860-679-2109, jlieberman@uchc.edu.

Conflict of Interest

Dr William C. Dougall is an employee of and owns stocks in Amgen Inc. All other authors state that they have no conflict of interest.

effective biologic therapy to inhibit the progression of established mixed lytic/blastic prostate cancer lesions in bone.

Introduction

Prostate adenocarcinoma is the most common malignancy in elderly men and there are estimated 217,730 new cases of prostate adenocarcinoma in the United States in year 2010 [1]. Bone is the most common site of metastasis from prostate adenocarcinoma and metastasis to bone results in increased morbidity, poor prognosis and decreased survival rate in prostate cancer patients [2,3]. Although prostate cancer is known to produce osteoblastic lesions in bone this probably represents a clinical continuum that also includes mixed lytic/blastic lesions [4]. The pathophysiology of the development of prostate cancer metastasis to bone remains poorly understood, and it has been difficult to identify effective treatment modalities.

Bone morphogenetic proteins (BMP) are members of the transforming growth factor beta (TGF-β) superfamily and play an integral role in endochondral ossification and bone repair [5,6]. BMPs also play a crucial role in embryogenesis and organogenesis by influencing proliferation, differentiation and migration of cellular targets [7]. Accordingly, BMPs were hypothesized as one of the candidate cytokines involved in the formation of bone metastasis. Aberrant BMP mRNA and protein expression has been found in human prostate cancer cell lines and in human biopsy specimens from bony metastatic sites [8–14]. BMP receptors have been found to be expressed on human prostate cancer cell lines and BMPs are known to regulate the expression of their receptors [13,15–17]. *In vitro* studies have demonstrated distinct effects of BMPs on proliferation, migration and invasion of tumor cells depending on the BMP type, the tumor cell lines and the bone microenvironment [13,15–20]. Noggin is a cysteine knot protein that inhibits BMP signal transduction by binding to BMPs and preventing them from binding to their corresponding receptors[21,22]. Priorp reclinical studies from our laboratory using human prostate cancer and human lung cancer cell lines in a mouse intratibial injection model have demonstrated that *in vivo* inhibition of BMP activity by noggin inhibits the development of osteoblastic lesions and diminishes the osteoblastic component in mixed lytic/blastic lesions in bone [13,23].

Local bone destruction is a significant aspect of many types of bony metastasis and is mediated via osteoclasts [4,24,25]. The RANK-RANKL (receptor activator of nuclear factor kappa-B) axis has been convincingly established as a key pathway regulating osteoclastogenesis in physiological as well as pathological conditions including bone metastasis [26–31]. The clinical success of bisphosphonates in reducing pain and skeletal related events (SRE) illustrates the significance of inhibiting osteoclasts in bone metastasis from prostate cancer [32–35]. Denosumab, which is a monoclonal antibody to RANKL, has shown significant promise in reducing SRE and markers of bone resorption in patients with metastatic bone disease [36]. Previous studies in our laboratory and others have investigated the influence of osteoclast depletion on establishment and progression of prostate cancer induced lesions in animal models of bone metastasis [23,37–42]. RANK-Fc, which is a recombinant RANKL antagonist, inhibited the osteolytic component and decreased the tumor growth in mixed lytic/blastic cancer lesions [23,37,38].

Once established in bone, the tumor cells interact with the bone microenvironment in a reciprocal fashion via cytokine mediators to form osteoblastic, osteolytic or mixed lytic/blastic lesions [43,44]. Although multiple cytokines are involved in the development of metastatic bone lesions, the exact interplay between these cytokines has not been established [45]. The development and progression of prostate cancer lesions in bone is known to be

influenced by the BMPs and RANKL but the interaction of these two cytokines in a mixed lytic/blastic prostate cancer lesion has not been studied in a preclinical model. In a previous study we noted that even when a predominantly osteoblastic lesion formed in bone, it was accompanied by an increase in osteoclasts [40]. The purpose of this study was to determine the influence of combined targeting of the RANKL and the BMP activity on the formation of mixed lytic/blastic prostate cancer lesions in a murine model of bone metastasis.

Materials and methods

Cell Line

The human prostate cancer cell line, C4 2b was used in this study. The C4 2b cell line is derived from the LNCaP cell line and forms mixed lytic/blastic lesions when injected in the long bones of immunecompromised mice [37,46–48]. The C4 2b cells were maintained in tissue culture in T medium (Invitrogen, Carlsbad, CA) with 10% fetal bovine serum (FBS) at 37°C in a humidified incubator with 5% of CO2 [48].

Retroviral vector production and transduction of prostate cancer cells

The retrovirus containing noggin cDNA was created according to a previously published protocol [13,49]. Briefly, the noggin cDNA was amplified with PCR and cloned into a murine leukemia virus-based retroviral vector pCLX at the *Not*I and *Bgl*II sites resulting in CLNog. The PCLX had been previously created from pLXSN (obtained originally from A Dusty Miller, Fred Hutchinson Cancer Research Center, Seattle, WA, USA) by removing the SV40 promoter and the neomycin resistance gene and replacing the U3 in the 5′ LTR with the human CMV promoter as described by Peng *et al* [50]. The CLNog vector DNA was converted into replication defective retrovirus by cotransfection with calcium phosphate precipitation into the GP-293 cell line (Clontech, Mountain view, CA) with a plasmid, pVSVG, which expressed vesicular stomatitis virus glycoprotein as the viral envelope. The conditioned medium containing the retrovirus (RN) was centrifuged at 3000rpm for 5 minutes to remove cellular debris and was stored at −80°C for future use.

For *ex vivo* transduction, the C4 2b cells were plated on a sterile culture dish in cell culture medium with 10% FBS. The cells were washed once with 1% PBS, and 2 ml fresh medium containing the retrovirus at an MOI of 100 was added to the cells. The virus was allowed to transduce the cells at 37°C, after which the virus containing media was removed. Geneticin (G418; Clontech Inc. Mountain view, CA) was used to select and maintain stable transfected C4 2b cell lines, which were used for the tibial injections. After transduction, the C4 2b cells were tested for the ability to express noggin with use of an in vitro BMP-4 inhibition alkaline phosphatase assay as previously described [13,23]. The retronoggin transduced cells on an average produced about 55ng/million cells/day of noggin.

RANK-Fc

The RANK-Fc used in this study was provided by Amgen Inc. (Thousand Oaks, CA). RANK-Fc is a recombinant RANKL antagonist formed by fusing the murine extracellular domain of RANK with Fc portion of human immunoglobulin G (IgG1). RANK-Fc was used in dose of 10 mg/kg dissolved in a 100 micro liter (μl) of phosphate buffer saline (PBS) and was injected subcutaneously three times a week.

Tibial implantation of prostate cancer cells

Eight week-old male severe combined immunodeficient (SCID) mice were housed under pathogen-free conditions in accordance with the protocol approved by the institutional Animal Research Committee (ARC). A murine intratibial injection model of bone metastasis was used to create bone lesions in this study as published previously [8,48]. The prostate

cancer cells (C4 2b; 5×10^5 cells) were suspended in 10 μl of 1% PBS and mixed with 10 μl of matrigel (BD biosciences, San Jose, CA) for each tibial injection. The prostate cancer cells were injected into the proximal tibia of 8 week-old SCID mice as published previously [39,48]. Briefly, the mice were anesthetized using 1.5–2 % isoflurane and oxygen in induction chamber. During the surgery, isoflurane and oxygen were delivered to the mice by a Bain circuit and nose cone adapter system. The wasteful gases were scavenged using the F/Air canister. The overlying skin was prepped in sterile fashion with 70% ethanol and betadine. A 3 millimeter (mm) longitudinal incision was made over the patellar ligament with a number 15 scalpel blade, and then a 2-mm longitudinal incision was made along the medial border of the patellar ligament to expose the tibial plateau. A 26 ½ gauge needle was introduced through the proximal tibial plateau and the prostate cancer cells were injected into the medullary cavity. The overlying skin incision was sutured and animals were allowed immediate weight bearing post operatively.

Study groups

In this study, forty five male SCID mice underwent tibial implantation with prostate cancer cells (C4 2b) and were divided into five study groups (Table 1). The untreated control group animals received prostate cancer cells (C4 2b) alone. The retronoggin treatment group (RN) animals received prostate cancer cells that were transduced *ex vivo* with a retroviral vector expressing noggin, which is a natural antagonist of BMPs. Animals in the empty vector control group (EV control) received prostate cancer cells that were transduced *ex vivo* with an empty retroviral vector which served as a control group to assess the potential influence of retroviral transduction on the biologic activity of the prostate cancer cells. The RANK-Fc treatment group animals received prostate cancer cells and three times a week subcutaneous injection of RANK-Fc (10mg/kg) for a total duration of 12 weeks. The combined treatment group animals (RN+RANK-Fc) received retroviral transduced prostate cancer cells expressing noggin (RN) and were also administered subcutaneous RANK-Fc (10mg/kg) three times a week for total duration of 12 weeks. Five animals in each study group underwent serial micro PET-CT at 4, 8 and 12 weeks and comprised the imaging subgroup. The time until animal sacrifice (12 weeks) was chosen on the basis of previously reported rates of growth and the size limitations of tumors established by the ARC at the author's institution [48]. Animals were sacrificed before 12 weeks if the soft-tissue tumor diameter reached 1.5 cm in any plane or if the animals showed signs of distress despite the maximum tumor diameter less than 1.5 cm. These measurements were chosen in accordance with regulations enforced by the ARC.

Hind limb tumor measurements

Hind limb tumor measurements in the tumor implanted tibias were recorded for all the animals in two bisecting planes with an electronic caliper at 4, 8 and 12 weeks. The soft tissue tumor burden was calculated from the hind limb measurements using the formula as described previously [48].

$$\text{Tumor volume} = (\text{length})\,(\text{width})^2 * 0.52$$

Radiographic analysis

The animals were anesthetized and radiographs were obtained using a Faxitron (Field Emission Corp., McMinnville, OR) at 4, 8 and 12 weeks animals as previously described [41,48]. The radiographs were analyzed for the presence of bony lesion and the type of bony lesion (osteoblastic, osteolytic or mixed lytic/blastic). Although previous studies from our laboratory and others have demonstrated a histologic evidence of osteoblastic component in

the mixed lesions formed by intratibial injection of C4 2b cells, radiographically they appear to have a predominant lytic component [46,48]. The mixed lytic/blastic lesions were radiographically characterized by thinning of the cortices, widening/ballooning of the proximal tibia, and presence of thin bony septa within the lesion. The radiographic appearance of osteoblastic lesions included loss of demarcation between the cortex and medullary cavity, narrow medullary canal, and increase radiodensity in the medullary cavity. The osteolytic lesions consisted of thinning of cortices and lucent areas in the cortex.

Radiotracer Preparation

Fluoride ion was produced using ^{18}O- water and proton bombardment using a RDS cyclotron (Siemens Preclinical solutions). ^{18}F-fluoride ion was produced at specific activities of approximately 1000 Ci/mmol and ^{18}F- fluorodeoxyglucose (FDG) was synthesized at specific activities of approximately 5000 mCi/mmol as previously described [48].

Micro PET-CT imaging protocol

The animals in the imaging subgroups (Table 1) underwent serial positron emission tomography (PET) scans and micro CT according to a previously published protocol [48]. Briefly, the mice were anesthetized with 1.5–2 % isoflurane and oxygen in induction chambers. The scavenging systems for the removal of wasteful gases included exhaust to outside air. The mice were then injected with approximately 250 μCi of ^{18}F-FDG tracer via tail vein using a 27 gauze needle on a tuberculin syringe. An hour later, whole-body scans were performed with a 10-minute acquisition time using a MicroPET®FOCUS 220 system (Siemens Preclinical Solutions). Immediately afterwards, a non-contrast enhanced microCT study using microCAT® II (Siemens Preclinical Solutions) imaging system was used to scan animals with a 10-minute acquisition time. PET scan images were reconstructed using filtered back projection and an iterative 3-dimensional reconstruction algorithm (maximum a posteriori [MAP]). MicroCT images were created using Fledkamp reconstruction at 200-μm resolution. MicroPET and microCAT images were then overlaid for analysis for use with AMIDE software [48]. The animals were injected with 250 μCi of ^{18}F-fluoride ion the next day using the same acquisition protocol.

Quantitative Analysis of micro PET-CT data

^{18}F-Fluoride and ^{18}F-FDG PET and CT data were analyzed and quantified by AMIDE (A Medical Image Data Examiner), version 0.7.154. ^{18}F- fluorodeoxyglucose (FDG) uptake correlates with the cellular glucose metabolism and was used in micro PET imaging for the detection and longitudinal monitoring of tumor burden as published previously [39,48]. Briefly, a region of interest (ROI) was drawn using a ROI box tool around the tumor implanted tibia, which was three-dimensionally reconstructed to confine the entire discernible FDG signal uptake. The maximum and mean intensity of the FDG signal uptake were then recorded within the tumor implanted tibias and the contralateral uninjected tibias using data analysis tools. The contralateral tibia was used as an internal control for each animal. To quantify the tumor size, FDG signal volume (mm^3) was calculated in the tumor implanted tibias. The FDG signal uptake in the contralateral tibia was used as the as the baseline control for this measurement. To quantify the fluoride activity in tibias, mean and maximum intensities of fluoride signal were recorded from the fixed ROIs drawn in both the tumor implanted tibias and the contralateral uninjected tibias. The maximum intensity of ^{18}F-Fluoride uptake in the uninjected contralateral tibia was used as a control in each animal. The fluoride activity in the injected tibia was expressed as percentage increase or decrease with respect to the internal control (contralateral tibia). The microCT images were used to identify and quantify the bone lesions. The microCT images were cropped (from top of the tibia to the ankle) to construct individual images of the implanted tibias and the

contralateral tibias. A standardized isocontour value was used to select the bone tissue and the bone volume was calculated as described previously [48]. The difference in the bone volume of the tumor implanted tibia and the contralateral tibia was calculated (ΔBV) to determine the changes in bone volume in the mixed lytic/blastic lesion [39,48].

Histology

After animal sacrifice, the tibias implanted with tumor cells were harvested for histologic examination and histomorphometric analysis. The hind limbs were amputated at the level of distal femur and ankle to harvest the specimen enblock. The harvested tibias were fixed in 10% buffered formalin overnight and followed by decalcification in 10% EDTA solution for 2 weeks at room temperature with gentle mechanical stirring. Following decalcification the samples were embedded in paraffin and saggital sections were obtained. The sections were stained with hematoxylin and eosin (H&E), orange G (OG) and tartrate-resistant acid phosphatase (TRAP) stains. Histomorphometric analysis was performed on an Olympus system (Olympus, Melville, NY) using the histomorphometric analysis software (Osteomeasure [Osteometrics, Decatur, GA]) as previously described [13,48]. Briefly, the number of osteoclasts per bone perimeter were calculated on TRAP stained histologic sections. The tumor induced new bone formation was quantified using the bone area to total area (BA/TA) in the medullary cavity on orange G stained sections.

Statistical analysis

The hind limb measurements, micro PET, micro CT, and histomorphometric data among different groups were compared using one way ANOVA analysis and a Post-hoc test (Newman Keuls multiple comparison test). P values < 0.05 were considered to be statistically significant.

Results

Plain radiographs demonstrate that combined treatment with RN and RANK-Fc inhibits development of mixed lytic/blastic lesions

The plain radiographs in the control groups (untreated control and EV control) demonstrated mixed lytic/blastic lesions involving most of the proximal half of tibia at 12 weeks after tumor cell injection (Fig. 1 and Table 2). The mixed lytic/blastic lesions were characterized by thinning of the cortices, widening of the medullary canal, and presence of thin bony septa within the lesion. The mixed lytic/blastic nature of these radiographic findings has been confirmed on histology by our laboratory and others previously [46,48]. The animals treated with RANK-Fc alone developed radiographic bony lesions in 5/9 animals at 12 weeks (Table 2). However, in contrast to the mixed lytic/blastic lesions seen in control group tibias, the osteolytic component was absent and the lesions were osteoblastic. The radiographic appearance of osteoblastic lesions included loss of demarcation between the cortex and medullary cavity, narrow medullary canal, and increase radiodensity in the medullary cavity. The radiographic lesions in the RN group were present in 5/10 animals. The bone lesions were smaller, limited to the proximal region of tibia and were characterized by a radiolucent defect in the cortex and thin cortices. The animals treated with both RN and RANK-Fc (combined treatment group) demonstrated bony lesions in only2/9 animals at 12 weeks and there was no osteolytic component in the bony lesions. There were no significant differences with respect to the presence of bone lesions on plain radiographs among all the study groups (p=0.09).

Combined treatment with RN and RANK-Fc limits skeletal tumor burden in the hind limbs

The skeletal tumor burden in the hind limbs was estimated from the hind limb measurements of tumor implanted tibias as described in the Methods section. The untreated control group and the EV control group animals developed soft tissue tumors in 7/10 and 4/5 tibias respectively at 12 weeks. Soft tissue tumors were present in 4/9 animals in the RANK-Fc group, 2/10 animals in the RN group and 2/9 animals in the combined treatment group (RN +RANK-Fc) at 12 weeks. The mean tumor sizes were significantly lower ($p<0.05$) in the combined treatment (RN+RANK-Fc) group animals (106 ± 34.5 mm^3) and the RN group animals (108.6 ± 21.6 mm^3) when compared to the control group animals (159.5 ± 43.4 mm^3). However, there were no significant differences ($p>0.05$) between the untreated control, EV control (146.9 ± 36.2 mm^3) controls and the RANK-Fc group (138.7 ± 54.8 mm^3) animals with respect to the mean tumor sizes at 12 weeks. Furthermore, there were no significant differences ($p>0.05$) amongst the RANK-Fc, the RN and the combined treatment group animals with respect to the mean tumor sizes.

Combined treatment with RN and RANK-Fc inhibits the lytic component of mixed lesions and prevents bone loss on serial microCT imaging

Serial micro CT scans were performed on the imaging subgroup animals at 4, 8 and 12 weeks in order to better define the bony lesions and study serial changes in the injected tibias with respect to bone loss or new bone formation. The difference (ΔBV)between the bone volume of the tumor implanted tibias and the bone volume of contralateral uninjected tibia was calculated to determine the bone loss in mixed lytic/blastic lesion at each time point(Fig. 2). Thinning of the cortices with cortical discontinuity was present on the reconstructed micro CT images in all the control group tibias(untreated controls and the EV control). Thinning of the cortices was also present in all but one of the tibias treated with RN alone. All the tibias in the RANK-Fc group and all but one tibia in the combined treatment group (RN + RANK-Fc) demonstrated thickening of the cortices, cortical irregularity with no cortical destruction or lytic lesion. The percentage increase in bone volume (ΔBV) in the RANK-Fc group tibias (17.2±4.4%)at 12 weeks was significantly higher when compared to RN group tibias($p<0.001$; −1.7±6.5%) and the RN+RANK-Fc group tibias ($p<0.05$;8.2 ± 4.7%). The ΔBV in the RN+RANK-Fc group was significantly higher($p<0.001$) when compared to the control group tibias and the RN treated tibias. There was an overall decrease in the ΔBV in injected tibias in the untreated control[−5.6±3.8%] and the EV control[−8.1±2%]and the RN group tibias at 12 weeks suggestive of overall bone loss.

Combined treatment with RN and RANK-Fc leads to decreased intraosseous tumor burden (^{18}F-FDG micro PET imaging)

^{18}F- fluorodeoxyglucose (FDG) uptake correlates with the cellular glucose metabolism and was used in micro PET imaging for the detection and longitudinal monitoring of tumor cells. There was an increased FDG uptake in the proximal portion of the injected tibias in the control groups (untreated control and EV control) and the RANK-Fc group animals when compared to the contralateral uninjected tibias at 4 week. In contrast, two (2/5) animals in the RN group and one (1/5) animal in the combined treatment group (RN+RANK-Fc) demonstrated maximum FDG signal intensity that was higher compared to contralateral uninjected tibias at 4 weeks. At 12 weeks all the injected tibias in the RN group and all but one animal in the combined treatment group demonstrated maximum signal intensity of FDG which was higher than the contralateral injected tibia (Fig. 3). The intraosseous and soft tissue tumor burden was calculated from the entire discernible FDG signal in the implanted tibia (FDG tumor size) as described in the Methods section. There was a progressive increase in the FDG tumor size at successive time points in all the study group animals (Fig. 4). Within each group, there were large variations in ^{18}F-FDG signal uptake in the tumors. The FDG tumor sizes at 12 weeks were lowest in the combined treatment group

animals (10.2±8 mm^3) but not significantly different from the animals in the RN group (29.5±25.8 mm^3), the RANK-Fc group and (139.9±140.6 mm^3) and the control groups (untreated control [118±102 mm^3] and EV control [109.5±74.4 mm^3]).

^{18}F-Fluoride micro PET

^{18}F-fluoride ion is a positron-emitting isotope with high affinity to bone. It has been shown to be preferentially deposited on the surface of the bone proportionate to the blood flow and bone remodeling [51]. There was increased uptake of fluoride tracer by all the growth plates including the one in upper tibia (Fig. 3). Increased uptake of the fluoride tracer by the growth plate in upper tibia limited the correct estimation and comparison of fluoride activity in the tumor implanted tibias. The maximum signal intensity of ^{18}F-fluoride tracer was recorded from the region of interest (ROI) drawn at a fixed distance away from the upper tibial growth plate in the tumor implanted tibias and the contralateral uninjected tibias. The ^{18}F-Fluoride uptake in the uninjected contralateral tibia was used as a control to calculate the change in fluoride activity (percentage increase) in the tumor implanted tibia. The percentage increase in the ^{18}F-fluoride activity in the RN group tibias (23.9±12.5) and the combined treatment group tibias (11.3±4) were significantly lower ($p<0.05$) than the control group tibias (untreated control [57.1±6.8] and EV control [39.2±9.8]) at 12 weeks. The percentage increase in the ^{18}F-fluoride uptake in injected tibias was not significantly different ($p>0.05$) in the RANK-Fc group tibias (45.1±7.6) compared to the control group tibias at 12 weeks. There was no significant differences ($p>0.05$) between injected tibias in the RN group when compared to the combined treatment group tibias with respect to the percentage increase in the maximum signal intensity of ^{18}F-fluoride tracer at 12 weeks.

Combined treatment with RN and RANK-Fc inhibits osteoclast mediated resorption of host bone and limits tumor induced new bone formation (histologic and histomorphometric analysis)

Histologic sections of the implanted tibias were stained with H&E, OG and TRAP to evaluate the changes occurring at the cellular level. The tibias in the control groups (untreated control and EV control) demonstrated thinning and destruction of the cortices and tumor cells present both within and outside the medullary canal (Fig. 5). Areas of new bone formation surrounded by the tumor cells were present in the medullary cavity and/or on the periosteal surface confirming the osteoblastic component in mixed bony lesions. The tibias in the RN group demonstrated tumor cells inside the medullary cavity with thinning of cortices and osteoclasts at the tumor-bone interface. In contrast to the control group animals, the tibias in the RANK-Fc group demonstrated new bone formation inside the medullary canal surrounded by the tumor cells which reflects the osteoblastic phenotype seen on radiographs (Fig. 5 and 6). There was no cortical bone destruction and osteoclasts were absent at the tumor-bone interface. In tibias treated with both RN and RANK-Fc (combined treatment group), the tumor cells were present in the medullary cavity mixed with some normal marrow elements. There was no cortical bone destruction and there was some tumor associated new bone formation present in the medullary canal.

The tumor associated new bone formed in the tibias was quantified and expressed as a percentage of total area (BA/TA) inside the medullary cavity to describe the influence of treatment on osteoblastic component of bone lesions (Fig 7). The BA/TA in the RANK-Fc group tibias (37.2±12.5) was significantly higher ($p<0.001$) than the RN+RANK-Fc group tibias (18±7), RN group tibias (3.3±2.7), and the control group tibias (untreated controls [12.4±3.5] and EV control [10.3±4.6]) (Fig. 7). The BA/TA was significantly lower in RN group tibias when compared to the control group ($p<0.05$) and RN+RANK-Fc group tibias ($p<0.01$).

The TRAP stained histologic sections were evaluated for qualitative and quantitative (number of osteoclasts per bone perimeter at tumor bone interface) assessment of osteoclasts in the study groups (Fig. 6 and Fig. 7). There were abundant osteoclasts present at the tumor bone interface in the control groups (untreated control [12.2±1.5 Oc/mm] and EV control [12.8±1.5 Oc/mm]) and RN group (10.3±2.7 OCs/mm). There were virtually no osteoclasts seen in the RANK-Fc group (0.3±0.5 OCs/mm) and the combined treatment group tibias (0.5±0.1 OCs/mm) tibias, and the number of osteoclasts at the tumor bone interface were significantly lower ($p<0.001$) than the control groups and the RN group tibias.

Discussion

A multitargeted approach that inhibits the complex interactions among the tumor cells and the bone microenvironment is required to effectively block the vicious cycle of bone metastasis [45,52–54]. Inhibition of multiple candidate cytokines that influence the cross talk among the tumor cells and the bone cells (osteoclasts and osteoblasts) is a novel way to delay the progression of established metastasis. This preclinical study demonstrates that the combined targeting of RANKL and BMP pathway in a mixed lytic/blastic prostate cancer lesion not only delays the progression of tumor and bone lesion formation but also prevents bone loss and preserves the bone architecture.

C4 2b is a LNCaP derived slow growing human prostate cancer cell line which forms mixed lytic/blastic lesions when implanted in the long bones of immunocompromised mice [46,48]. Treatment of C4 2b implanted tibias with RANK-Fc alone, which is a RANKL antagonist and inhibits the formation, function and survival of osteoclasts, abolished the osteolytic component in the mixed lytic/blastic lesion as demonstrated by the radiographs, micro CT, histologic and histomorphometric data. In a preclinical study using an intratibial injection model, Ignatoski *et al* reported complete inhibition of osteolysis and increased bone mineral density in C4 2b implanted tibias treated with RANK-Fc, which is consistent with the results in our study. In the present study, C4 2b implanted tibias treated with RANK-Fc alone demonstrated an osteoblastic phenotype on plain radiographs and there was new pathological bone surrounded by tumor cells on histologic sections. We hypothesize that the osteoblastic pathway is not interrupted with RANK-Fc treatment in a mixed lytic/blastic lesion and hence the tumor associated new bone formation continues inside the medullary canal and/or on the extra cortical surface and is indicative of residual tumor induced osteoblastic activity. We have previously demonstrated that in a pure osteolytic prostate cancer cell line (PC-3), treatment with RANK-Fc prevents tumor associated osteolysis but does not result in tumor associated new bone formation. These results suggest that the cytokine profile of tumor cells is a critical element in determining their biologic behavior when these cells metastasize to bone. In a SCID mouse intratibial injection model, Feeley *et al* demonstrated that treatment of a mixed lytic/blastic lung cancer lesion with RANK-Fc produced tumors with a pure osteoblastic phenotype which is similar to the results in this study with a mixed lytic/blastic prostate cancer bone lesion. Inhibition of one component in a mixed lytic/blastic lesion leads to more obvious persistence of the remaining component. Although, many tumors are predominantly osteoblastic or osteolytic in radiographic appearance they will occasionally have lytic or blastic activity respectively, which needs to be addressed in order to achieve complete or maximal inhibition of bone lesion.

RANK-Fc does not directly inhibit tumor growth. We and others have previously demonstrated that RANK-Fc administration does not inhibit tumor growth in a subcutaneous xenograft tumor model. However, in an intratibial injection model of bone metastasis RANK-Fc inhibits tumor mediated osteolysis and indirectly limits tumor growth by preventing the release of growth promoting factors from bone [23,37–39,41,55].

Inhibition of BMPs by noggin over expression in C4 2b cells suppressed the osteoblastic component in a mixed lesion and lead to formation of smaller lesions with an osteolytic phenotype as demonstrated on plain radiographs, micro CT and histomorphometric data. Schwaninger *et al* using a similar animal model demonstrated that noggin over expression in C4 2b cells abolished their osteoblastic response when injected in tibia of an immune compromised mice, which is consistent with the findings in this study [56]. In another study using intratibial injection model in SCID mice, Hall *et al* demonstrated that inhibition of osteoblastic activity in C4 2b induced mixed lytic/blastic lesions transformed them into osteolytic tumors [46]. Clearly, the aforementioned studies and the current study highlight the fact that suppression of an osteoblastic pathway in a mixed bone lesion results in a residual osteolytic phenotype.

BMPs have previously been shown to influence cell proliferation and cellular growth in prostate cancer [13,15,16,19]. We have previously demonstrated that BMPs stimulate invasion and migration of prostate cancer cells *in vitro* and these effects can be reversed with addition of noggin [13]. In this study, noggin mediated inhibition of BMPs in C4 2b tumors resulted in smaller tumors as compared to untreated controls as demonstrated on FDG micro PET scans and hind limb tumor measurements. Noggin did not demonstrate any significant effect on osteoclast formation as demonstrated on histologic assessment. Mixed results have been reported previously regarding the influence of noggin on osteoclast activity and formation. Feeley *et al* demonstrated that noggin prevents osteoclastic activity *in vitro* but did not affect osteoclast formation *in vivo* [49]. Schwaninger *et al* demonstrated that noggin possesses antiresorption activity and inhibited osteoclast formation both *in vitro* and *in vivo* [56]. Smaller osteolytic bone lesions in C4 2b tumors treated with retronoggin treatment in this study are most likely due to smaller tumor burden with inhibition of osteoblastic pathway.

It is our hypothesis that in a mixed lytic/blastic lesion, specific targeting of either the pro-osteoblastic or the pro-osteoclast pathways can diminish the progression of a mixed lesion but complete inhibition would require simultaneous blockade of both the components. In fact, the skeletal complications including pathologic fractures associated with advanced metastatic prostate cancer are thought to be due to both osteolysis as well as disorganized new bone formation that is under mineralized and biomechanically weak [57]. The RANK-RANKL pathway, which is activated by the cytokines secreted by the tumor cells (IL-8, IL-11, PTHrP) as well as by the tumor induced osteoblastic activity, is inhibited by the RANK-Fc treatment that suppresses the osteolytic component in a mixed lytic/blastic lesion [58]. Noggin blocks the effect of local BMPs which are one of candidate cytokines postulated in formation of osteoblastic lesions [44,58,59]. In this study combined treatment with retronoggin and RANK-Fc prevented bone loss, limited the osteoblastic component in mixed lytic/blastic lesion and resulted in smaller soft tissue tumor sizes. Mixed lytic/blastic lesions formed by C4 2b cells in the SCID mice are characterized by predominant osteolytic and minor osteoblastic component as demonstrated by the radiographs, micro CT and histology. In animals treated with both retronoggin and RANK-Fc, noggin did not completely inhibit the overt osteoblastic response. This could be due to incomplete noggin inhibition of the cells via the retroviral transduction or due to the presence of other uninhibited pro-osteoblastic cytokines such as endothelin-1 and Wnts [46,59].

Our laboratory and others have previously demonstrated that micro PET-CT can be a useful tool in assessing tumor growth and changes in bone turnover in pure osteolytic and osteoblastic prostate cancer lesions in murine intra tibial injection model [39,48,60]. However, there are limitations with the use of ^{18}F-Fluoride and ^{18}F-FDG micro PET for C4 2b induced mixed lytic/blastic lesions in mice tibia. We have previously demonstrated that uptake of ^{18}F-Fluoride, which is preferentially deposited in areas of bone turnover, is

diminished in osteolytic lesions because these lesions are characterized by bone destruction [39]. Consequently, the presence of both osteolytic component limits accurate assessment of osteoblastic activity in mixed lytic/blastic lesions with fluoride micro PET [48]. Moreover, uptake of fluoride tracer by the growth plate in a mouse tibia interferes with accurate estimation of signal uptake associated with tumor induced osteoblastic activity especially at early time points when the tumor is limited to the upper tibia. There was high variability of FDG tracer uptake by the C4 2b tumor cells within study groups and individual tumors, a finding which is consistent with a previous study in our laboratory with C4 2b tumors in a mouse intratibial model [48]. This could be due to tumor necrosis secondary to poor blood supply or due to abnormal cellular metabolism in the C4 2b cells at later stages of tumor growth.

Metastatic bone lesions represent a continuum that includes osteoblastic, mixed lytic/blastic and osteolytic lesions, which are a consequence of dysregulation of the normal bone remodeling process that is induced by the factors released by the tumor cells in the bone microenvironment [43–45]. It is interesting that mixed lesions produced by prostate and lung cancer cells respond in a similar fashion to the combination therapy. We are presently analyzing the cytokine production of different tumor cell populations in order to identify the critical candidates that determine the type of bone lesion that is produced. This data suggests that the type of therapy developed to treat metastatic disease should take into account the cytokine profile of the tumor cells and the radiographic phenotype of the lesion that it produces. Clearly, single blanket treatment may not work for all types of metastatic lesions. In a prior preclinical study, we noted that the human osteoblastic prostate cancer cell line, LAPC-9 induced both bone formation and then osteoclastic activation in the intratibial injection model [13,40]. It was our hypothesis that the osteoclast activity that occurred in response to the new bone promoted further tumor cell proliferation. The data from our laboratory and others analyzing osteolytic, osteoblastic and mixed lesions using preclinical studies suggest that a combination approach of targeting both osteoblasts and osteoclasts may have benefit in limiting the progression of established bone metastasis. The results of this study suggest that systemic inhibition of osteoclasts and local BMP inhibition via intralesional injection could be used as a minimally invasive therapy in prostate cancer patients with metastatic disease to bone and should be tested in clinical trials. We hypothesize that RANK-Fc will prevent the skeletal complications that occur secondary to osteolysis and noggin will limit the progression of bone metastasis.

Research Highlights

- Treatment with RANK-Fc alone inhibited osteolysis and transformed a mixed lytic/blastic lesion into an osteoblastic phenotype.
- Inhibition of local BMPs inhibited the osteoblastic component in a mixed lytic/blastic lesion and resulted in formation of smaller osteolytic bone lesion with smaller soft tissue size.
- Combined treatment with both RANK-Fc and retronoggin (BMP antagonist) demonstrated delayed development of bone lesions, inhibition of osteolysis, small soft tissue tumors and preservation of bone architecture with less tumor induced new bone formation.

Acknowledgments

This work was supported by a research grant from the National Institute of Health (RO1 CA103039 to JRL).

RANK-Fc was generously provided by Amgen Inc

References

1. Jemal, A.; Siegel, R.; Xu, J.; Ward, E. CA Cancer J Clin. 2010. Cancer Statistics.
2. Mundy GR. Metastasis to bone: causes, consequences and therapeutic opportunities. Nat Rev Cancer 2002;2:584–93. [PubMed: 12154351]
3. Coleman RE. Clinical features of metastatic bone disease and risk of skeletal morbidity. Clin Cancer Res 2006;12:6243s–6249s. [PubMed: 17062708]
4. Roudier MP, Morrissey C, True LD, Higano CS, Vessella RL, Ott SM. Histopathological assessment of prostate cancer bone osteoblastic metastases. J Urol 2008;180:1154–60. [PubMed: 18639279]
5. Lieberman JR, Daluiski A, Einhorn TA. The role of growth factors in the repair of bone. Biology and clinical applications. J Bone Joint Surg Am 2002;84-A:1032–44. [PubMed: 12063342]
6. Chen D, Zhao M, Mundy GR. Bone morphogenetic proteins. Growth Factors 2004;22:233–41. [PubMed: 15621726]
7. Li X, Cao X. BMP signaling and skeletogenesis. Ann N Y Acad Sci 2006;1068:26–40. [PubMed: 16831903]
8. Lee Y, Schwarz E, Davies M, Jo M, Gates J, Wu J, Zhang X, Lieberman JR. Differences in the cytokine profiles associated with prostate cancer cell induced osteoblastic and osteolytic lesions in bone. J Orthop Res 2003;21:62–72. [PubMed: 12507581]
9. Bobinac D, Maric I, Zoricic S, Spanjol J, Dordevic G, Mustac E, Fuckar Z. Expression of bone morphogenetic proteins in human metastatic prostate and breast cancer. Croat Med J 2005;46:389–96. [PubMed: 15861517]
10. Brubaker KD, Corey E, Brown LG, Vessella RL. Bone morphogenetic protein signaling in prostate cancer cell lines. J Cell Biochem 2004;91:151–60. [PubMed: 14689587]
11. Autzen P, Robson CN, Bjartell A, Malcolm AJ, Johnson MI, Neal DE, Hamdy FC. Bone morphogenetic protein 6 in skeletal metastases from prostate cancer and other common human malignancies. Br J Cancer 1998;78:1219–23. [PubMed: 9820184]
12. Masuda H, Fukabori Y, Nakano K, Takezawa Y, TCS, Yamanaka H. Increased expression of bone morphogenetic protein-7 in bone metastatic prostate cancer. Prostate 2003;54:268–74. [PubMed: 12539225]
13. Feeley BT, Gamradt SC, Hsu WK, Liu N, Krenek L, Robbins P, Huard J, Lieberman JR. Influence of BMPs on the formation of osteoblastic lesions in metastatic prostate cancer. J Bone Miner Res 2005;20:2189–99. [PubMed: 16294272]
14. Harris SE, Harris MA, Mahy P, Wozney J, Feng JQ, Mundy GR. Expression of bone morphogenetic protein messenger RNAs by normal rat and human prostate and prostate cancer cells. Prostate 1994;24:204–11. [PubMed: 8146069]
15. Yang S, Zhong C, Frenkel B, Reddi AH, Roy-Burman P. Diverse biological effect and Smad signaling of bone morphogenetic protein 7 in prostate tumor cells. Cancer Res 2005;65:5769–77. [PubMed: 15994952]
16. Ide H, Yoshida T, Matsumoto N, Aoki K, Osada Y, Sugimura T, Terada M. Growth regulation of human prostate cancer cells by bone morphogenetic protein-2. Cancer Res 1997;57:5022–7. [PubMed: 9371496]
17. Ye L, Lewis-Russell JM, Kyanaston HG, Jiang WG. Bone morphogenetic proteins and their receptor signaling in prostate cancer. Histol Histopathol 2007;22:1129–47. [PubMed: 17616940]
18. Ye L, Kynaston H, Jiang WG. Bone morphogenetic protein-10 suppresses the growth and aggressiveness of prostate cancer cells through a Smad independent pathway. J Urol 2009;181:2749–59. [PubMed: 19375725]
19. Morrissey C, Brown LG, Pitts TE, Vessella RL, Corey E. Bone morphogenetic protein 7 is expressed in prostate cancer metastases and its effects on prostate tumor cells depend on cell phenotype and the tumor microenvironment. Neoplasia 12:192–205. [PubMed: 20126477]
20. Dai J, Keller J, Zhang J, Lu Y, Yao Z, Keller ET. Bone morphogenetic protein-6 promotes osteoblastic prostate cancer bone metastases through a dual mechanism. Cancer Res 2005;65:8274–85. [PubMed: 16166304]

21. Rosen V. BMP and BMP inhibitors in bone. Ann N Y Acad Sci 2006;1068:19–25. [PubMed: 16831902]
22. Groppe J, Greenwald J, Wiater E, Rodriguez-Leon J, Economides AN, Kwiatkowski W, Affolter M, Vale WW, Belmonte JC, Choe S. Structural basis of BMP signalling inhibition by the cystine knot protein Noggin. Nature 2002;420:636–42. [PubMed: 12478285]
23. Feeley BT, Liu NQ, Conduah AH, Krenek L, Roth K, Dougall WC, Huard J, Dubinett S, Lieberman JR. Mixed metastatic lung cancer lesions in bone are inhibited by noggin overexpression and Rank:Fc administration. J Bone Miner Res 2006;21:1571–80. [PubMed: 16995812]
24. Roodman GD, Dougall WC. RANK ligand as a therapeutic target for bone metastases and multiple myeloma. Cancer Treat Rev 2008;34:92–101. [PubMed: 17964729]
25. Keller ET. The role of osteoclastic activity in prostate cancer skeletal metastases. Drugs Today (Barc) 2002;38:91–102. [PubMed: 12532187]
26. Lacey DL, Timms E, Tan HL, Kelley MJ, Dunstan CR, Burgess T, Elliott R, Colombero A, Elliott G, Scully S, Hsu H, Sullivan J, Hawkins N, Davy E, Capparelli C, Eli A, Qian YX, Kaufman S, Sarosi I, Shalhoub V, Senaldi G, Guo J, Delaney J, Boyle WJ. Osteoprotegerin ligand is a cytokine that regulates osteoclast differentiation and activation. Cell 1998;93:165–76. [PubMed: 9568710]
27. Yasuda H, Shima N, Nakagawa N, Yamaguchi K, Kinosaki M, Mochizuki S, Tomoyasu A, Yano K, Goto M, Murakami A, Tsuda E, Morinaga T, Higashio K, Udagawa N, Takahashi N, Suda T. Osteoclast differentiation factor is a ligand for osteoprotegerin/osteoclastogenesis-inhibitory factor and is identical to TRANCE/RANKL. Proc Natl Acad Sci U S A 1998;95:3597–602. [PubMed: 9520411]
28. Dougall WC, Chaisson M. The RANK/RANKL/OPG triad in cancer-induced bone diseases. Cancer Metastasis Rev 2006;25:541–9. [PubMed: 17180711]
29. Hofbauer LC, Neubauer A, Heufelder AE. Receptor activator of nuclear factor-kappaB ligand and osteoprotegerin: potential implications for the pathogenesis and treatment of malignant bone diseases. Cancer 2001;92:460–70. [PubMed: 11505389]
30. Michigami T, Ihara-Watanabe M, Yamazaki M, Ozono K. Receptor activator of nuclear factor kappaB ligand (RANKL) is a key molecule of osteoclast formation for bone metastasis in a newly developed model of human neuroblastoma. Cancer Res 2001;61:1637–44. [PubMed: 11245477]
31. Kitazawa S, Kitazawa R. RANK ligand is a prerequisite for cancer-associated osteolytic lesions. J Pathol 2002;198:228–36. [PubMed: 12237883]
32. Higano CS. Understanding treatments for bone loss and bone metastases in patients with prostate cancer: a practical review and guide for the clinician. Urol Clin North Am 2004;31:331–52. [PubMed: 15123412]
33. Eaton CL, Coleman RE. Pathophysiology of bone metastases from prostate cancer and the role of bisphosphonates in treatment. Cancer Treat Rev 2003;29:189–98. [PubMed: 12787713]
34. Hatoum HT, Lin SJ, Smith MR, Barghout V, Lipton A. Zoledronic acid and skeletal complications in patients with solid tumors and bone metastases: analysis of a national medical claims database. Cancer 2008;113:1438–45. [PubMed: 18720527]
35. Saad F. Clinical benefit of zoledronic acid for the prevention of skeletal complications in advanced prostate cancer. Clin Prostate Cancer 2005;4:31–7. [PubMed: 15992459]
36. Body JJ, Lipton A, Gralow J, Steger GG, Gao G, Yeh H, Fizazi K. Effects of Denosumab in Patients with Bone Metastases, with and without Previous Bisphosphonate Exposure. J Bone Miner Res. 2009
37. Ignatoski KM, Escara-Wilke JF, Dai JL, Lui A, Dougall W, Daignault S, Yao Z, Zhang J, Day ML, Sargent EE, Keller ET. RANKL inhibition is an effective adjuvant for docetaxel in a prostate cancer bone metastases model. Prostate 2008;68:820–829. [PubMed: 18324676]
38. Zhang J, Dai J, Yao Z, Lu Y, Dougall W, Keller ET. Soluble receptor activator of nuclear factor kappaB Fc diminishes prostate cancer progression in bone. Cancer Res 2003;63:7883–90. [PubMed: 14633717]
39. Virk MS, Petrigliano FA, Liu NQ, Chatziioannou AF, Stout D, Kang CO, Dougall WC, Lieberman JR. Influence of simultaneous targeting of the bone morphogenetic protein pathway and RANK/

RANKL axis in osteolytic prostate cancer lesion in bone. Bone 2009;44:160–7. [PubMed: 18929692]

40. Lee YP, Schwarz EM, Davies M, Jo M, Gates J, Zhang X, Wu J, Lieberman JR. Use of zoledronate to treat osteoblastic versus osteolytic lesions in a severe-combined-immunodeficient mouse model. Cancer Res 2002;62:5564–70. [PubMed: 12359769]
41. Whang PG, Schwarz EM, Gamradt SC, Dougall WC, Lieberman JR. The effects of RANK blockade and osteoclast depletion in a model of pure osteoblastic prostate cancer metastasis in bone. J Orthop Res 2005;23:1475–83. [PubMed: 16005175]
42. Miller RE, Roudier M, Jones J, Armstrong A, Canon J, Dougall WC. RANK ligand inhibition plus docetaxel improves survival and reduces tumor burden in a murine model of prostate cancer bone metastasis. Mol Cancer Ther 2008;7:2160–9. [PubMed: 18606716]
43. Guise TA, Mohammad KS, Clines G, Stebbins EG, Wong DH, Higgins LS, Vessella R, Corey E, Padalecki S, Suva L, Chirgwin JM. Basic mechanisms responsible for osteolytic and osteoblastic bone metastases. Clin Cancer Res 2006;12:6213s–6216s. [PubMed: 17062703]
44. Roodman GD. Mechanisms of bone metastasis. N Engl J Med 2004;350:1655–64. [PubMed: 15084698]
45. Virk MS, Lieberman JR. Tumor metastasis to bone. Arthritis Res Ther 2007;9 (Suppl 1):S5. [PubMed: 17634144]
46. Hall CL, Bafico A, Dai J, Aaronson SA, Keller ET. Prostate cancer cells promote osteoblastic bone metastases through Wnts. Cancer Res 2005;65:7554–60. [PubMed: 16140917]
47. Thalmann GN, Sikes RA, Wu TT, Degeorges A, Chang SM, Ozen M, Pathak S, Chung LW. LNCaP progression model of human prostate cancer: androgen-independence and osseous metastasis. Prostate 2000 Jul 1;44(2):91–103. [PubMed: 10881018]
48. Hsu WK, Virk MS, Feeley BT, Stout DB, Chatziioannou AF, Lieberman JR. Characterization of Osteolytic, Osteoblastic, and Mixed Lesions in a Prostate Cancer Mouse Model with Using 18F-FDG and 18F-Fluoride PET/CT. J Nucl Med. 2008
49. Feeley BT, Krenek L, Liu N, Hsu WK, Gamradt SC, Schwarz EM, Huard J, Lieberman JR. Overexpression of noggin inhibits BMP-mediated growth of osteolytic prostate cancer lesions. Bone 2006;38:154–66. [PubMed: 16126463]
50. Peng H, Chen ST, Wergedal JE, Polo JM, Yee JK, Lau KH, Baylink DJ. Development of an MFG-based retroviral vector system for secretion of high levels of functionally active human BMP4. Mol Ther 2001;4:95–104. [PubMed: 11482980]
51. Hawkins RA, Choi Y, Huang SC, Hoh CK, Dahlbom M, Schiepers C, Satyamurthy N, Barrio JR, Phelps ME. Evaluation of the skeletal kinetics of fluorine-18-fluoride ion with PET. J Nucl Med 1992;33:633–42. [PubMed: 1569473]
52. Loberg RD, Gayed BA, Olson KB, Pienta KJ. A paradigm for the treatment of prostate cancer bone metastases based on an understanding of tumor cell-microenvironment interactions. J Cell Biochem 2005;96:439–46. [PubMed: 15988761]
53. Vessella RL, Corey E. Targeting factors involved in bone remodeling as treatment strategies in prostate cancer bone metastasis. Clin Cancer Res 2006;12:6285s–6290s. [PubMed: 17062715]
54. Canon J, Bryant R, Roudier M, Osgood T, Jones J, Miller R, Coxon A, Radinsky R, Dougall WC. Inhibition of RANKL increases the anti-tumor effect of the EGFR inhibitor panitumumab in a murine model of bone metastasis. Bone.
55. Holland PM, Miller R, Jones J, Douangpanya H, Piasecki J, Roudier M, Dougall WC. Combined therapy with the RANKL inhibitor RANK-Fc and rhApo2L/TRAIL/dulanermin reduces bone lesions and skeletal tumor burden in a model of breast cancer skeletal metastasis. Cancer Biol Ther :9.
56. Schwaninger R, Rentsch CA, Wetterwald A, van der Horst G, van Bezooijen RL, van der Pluijm G, Lowik CW, Ackermann K, Pyerin W, Hamdy FC, Thalmann GN, Cecchini MG. Lack of noggin expression by cancer cells is a determinant of the osteoblast response in bone metastases. Am J Pathol 2007;170:160–75. [PubMed: 17200191]
57. Saad F, Clarke N, Colombel M. Natural history and treatment of bone complications in prostate cancer. Eur Urol 2006;49:429–40. [PubMed: 16431012]

58. Chirgwin JM, Mohammad KS, Guise TA. Tumor-bone cellular interactions in skeletal metastases. J Musculoskelet Neuronal Interact 2004;4:308–18. [PubMed: 15615499]

59. Guise TA, Yin JJ, Mohammad KS. Role of endothelin-1 in osteoblastic bone metastases. Cancer 2003;97:779–84. [PubMed: 12548575]

60. Berger F, Lee YP, Loening AM, Chatziioannou A, Freedland SJ, Leahy R, Lieberman JR, Belldegrun AS, Sawyers CL, Gambhir SS. Whole-body skeletal imaging in mice utilizing microPET: optimization of reproducibility and applications in animal models of bone disease. Eur J Nucl Med Mol Imaging 2002;29:1225–36. [PubMed: 12418463]

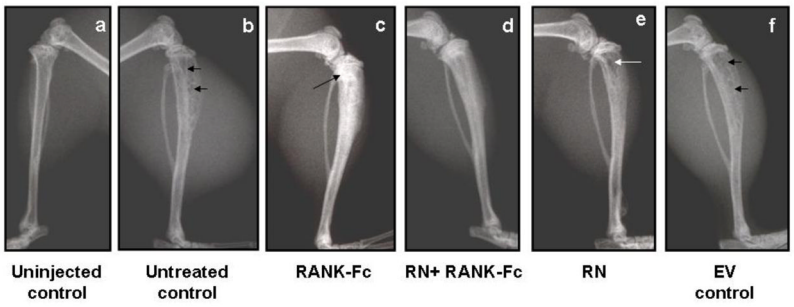

Fig. 1. Plain Radiographs at 12 weeks

C4 2b cells form mixed lytic/blastic lesions, which are characterized by thin cortices, widened medullary canal and strands of bone tissue within the lesion (untreated control group; double black arrows in image b). Treatment with RANK-Fc alone inhibited the osteolytic component of a mixed lytic/blastic lesion and resulted in an osteoblastic phenotype characterized by loss of demarcation between the cortex and medullary cavity, narrow medullary canal, and increase radiodensity in the medullary cavity (black arrow in image c). Animals injected with C4 2b cells that were transduced with retronoggin (RN group) formed osteolytic lesions that were small (white arrow in image e). Radiographs of the implanted tibias treated with both RANK-Fc and RN (image d) demonstrated no osteolysis (intact cortices) with relatively preserved architecture of the tibia compared to the uninjected contralateral control tibia (image a). The radiographs of tibias injected with C4 2b cells that were transduced with empty vector (Empty vector control; image f) were similar to the untreated controls.

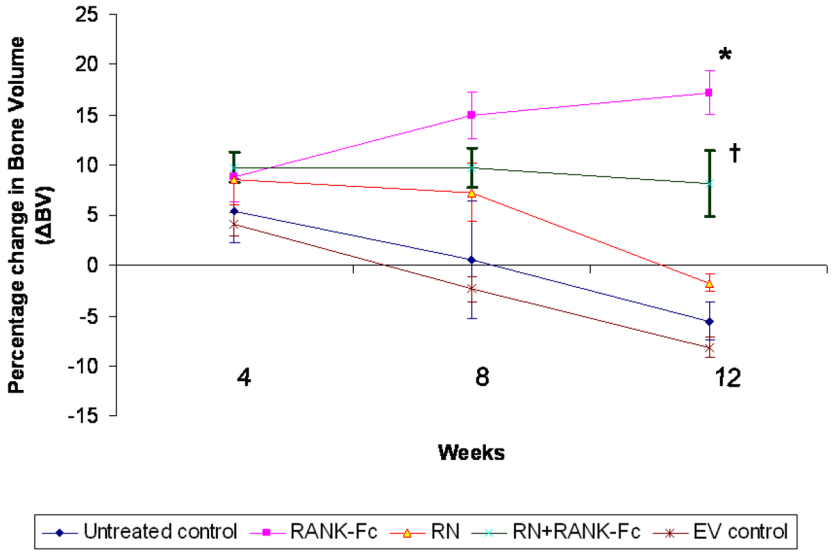

*p<0.05 vs. RN+RANK-Fc; p<0.001 vs. Untreated control, EV control, RN
†p<0.001 vs. RN

Fig. 2. Serial monitoring of changes in bone volume (ΔBV)with micro CT in study groups

The ΔBV in the RANK-Fc group tibias at 12 weeks was significantly higher than the combined treatment group (p<0.05), the RN group (p<0.001) and the control group (p<0.001)tibias. The ΔBV in RN+RANK-Fc tibias was significantly higher (p<0.001) than the RN treatment group tibias. There was overall bone loss in the control groups (untreated control and EV control) and the RN group tibias at 12 weeks as demonstrated by the negative ΔBV.

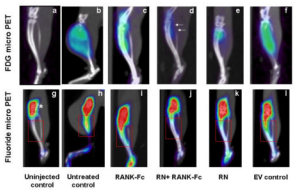

Fig. 3.

^{18}F- fluorodeoxyglucose (top panel) and ^{18}F-fluoride (bottom panel) micro PET-CT Top Panel (a–f): ^{18}F- fluorodeoxyglucose (FDG) which correlates with cellular glucose metabolism demonstrated increased uptake by the tumor tissue in study groups at 12 weeks. The FDG uptake was lowest in animals treated with RN+RANK-Fc (white arrows in d) compared to the other treatment group animals. There were large variations in the FDG uptake in C4 2b tumors in all the groups. Bottom panel (g–i): ^{18} F-fluoride which correlates with the bone turnover shows increased uptake in all the injected tibias. Uptake of fluoride tracer by the growth plate (uninjected control tibia; asterisk in g) limits correct estimation of uptake of fluoride tracer in the proximal tibia in this animal model. However, increased uptake of fluoride tracer was seen in untreated control, EV control and RANK-Fc tibias extending up to the middle third of the tibias (red boxes in h, i and l) compared to the RN and RN+RANK-Fc tibias (red boxes in j and k) where it was limited to the upper tibia.

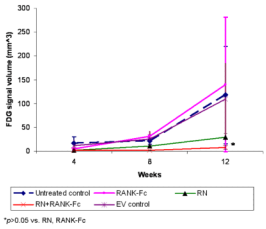

Fig. 4. Serial estimation of tumor volume using ^{18}F- fluorodeoxyglucose (FDG) micro PET in the study groups at 4, 8 and 12 weeks

There was a progressive increase in the FDG tumor size at successive time points in all the study group animals. The FDG tumor sizes at 12 weeks were lowest in the combined treatment group animals (10.2±8 mm^3) but not significantly different from the animals in the RN group (29.5±25.8 mm^3), the RANK-Fc group and (139.9±140.6 mm^3) and the control groups (untreated control [118±102 mm^3] and EV control [109.5±74.4 mm^3]).

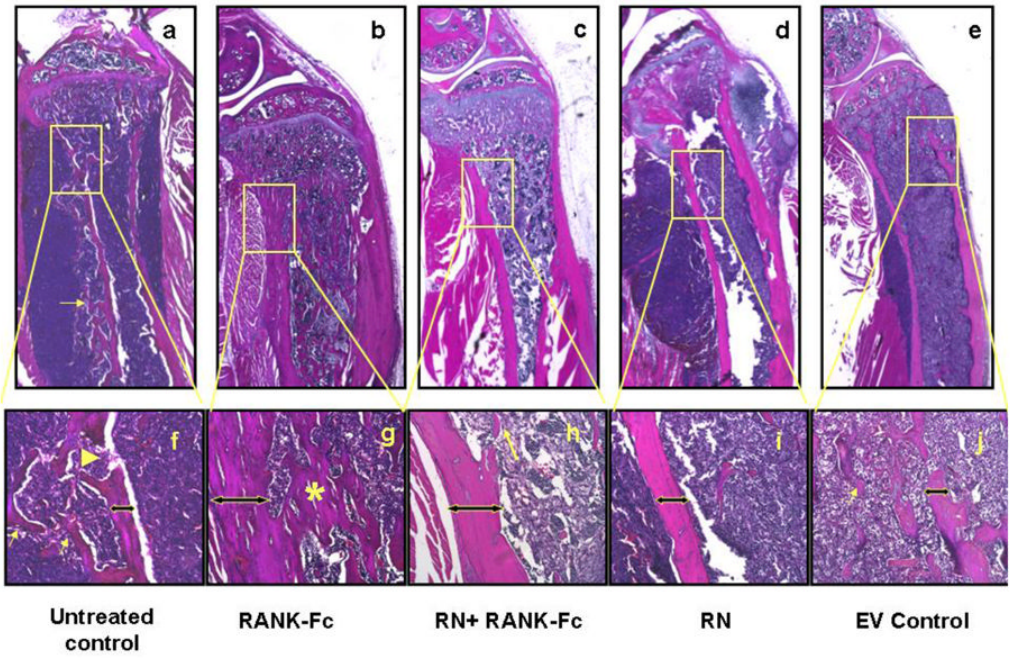

Fig. 5. Histologic sections of injected tibias in the study groups (top panel: images a–e, 1x magnification; bottom panel: images f–j, 10 x magnifications)

Untreated control (images a & f) and EV control (images e & j) tibias demonstrate both new bone formation (thin yellow arrows in f & j) and osteolysis (cortical break [yellow arrow head in image f] and thin cortices [left right arrow in image f &j]). The tibias treated with RANK-Fc alone (images b & g) demonstrated intact and thick cortices (left right arrow in image g) and abundant new bone formation in the medullary canal (asterisk in image g) surrounded by tumor cells. The RN treated tibias (images d & i) show thinning of cortices and minimal new bone formation in the medullary canal. The RN+RANK-Fc treatment group tibias (combined treatment group; images c & h) demonstrate intact cortices with some new bone formation in the medullary canal (thin yellow arrow in image h).

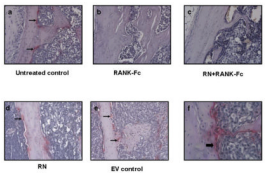

Fig. 6.

Histology (TRAP stain; 20x magnification) of implanted tibias in the study groups RANK-Fc is a recombinant RANKL antagonist that blocks formation, function and survival of osteoclasts. Injected tibias of animals treated with RANK-Fc ([RANK-Fc group; image b] and RN+RANK-Fc group [image c]) demonstrate minimal to no osteoclasts on TRAP stain. In contrast, injected tibias in untreated control (image a), EV control (image e) and animals treated with RN (image d) have abundant osteoclasts at the tumor bone interface (black arrows). Image f is a higher magnification image (40x) demonstrating multinucleate appearance of active osteoclasts.

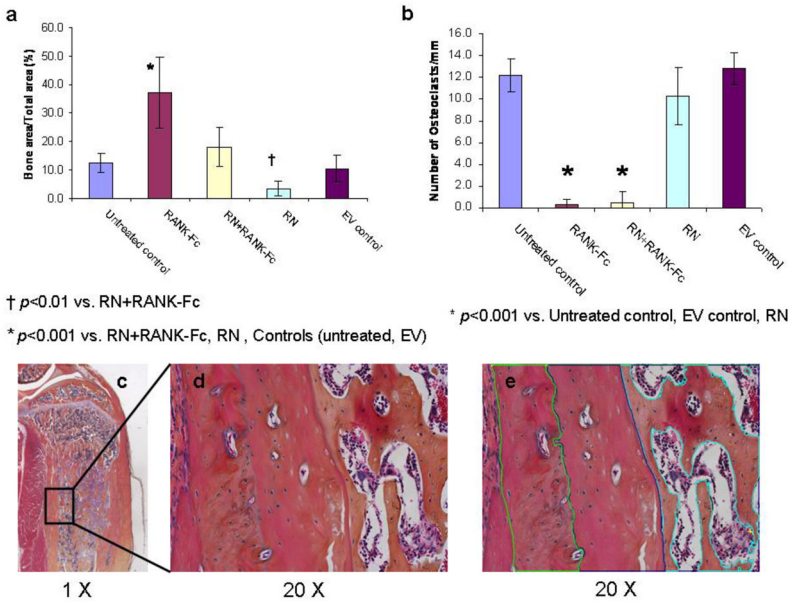

Fig. 7. Histomorphometry

The tumor induced new bone formed in the injected tibias was quantified using bone area/total area (BA/TA) inside the medullary cavity (a). The BA/TA in the RANK-Fc tibias (37.2±12.5) was significantly higher ($p<0.001$) than the RN+RANK-Fc(18±7), RN (3.3±2.7), untreated control (11.8±4) and EV control (9.3±4.6) tibias. The BA/TA was significantly lower in RN tibias ($p<0.01$) when compared to the RN+RANK-Fc tibias. B. The number of osteoclasts per mm of bone perimeter at the tumor-host bone interface was quantified to study the effect of RANK-Fc on osteoclasts. The number of osteoclasts/mm were significantly lower ($p<0.001$) in the tibias treated with RANK-Fc (RANK-Fc group and RN+RANK-Fc group) compared to tibias not treated with RANK-Fc (untreated control, EV control and RN group). Image c (1 x image), image d (20 X image) and image e (green highlighting extracortical new bone; blue highlighting host original cortex; turquoise highlighting intramedullary new bone formation) demonstrating the regions used for BA evaluation during histomorphometric analysis. Tumor associated intramedullary new bone (outlined in turquoise color in image e) was measured at 20X magnification on orange G stained histologic slides to measure BA.

Table 1

Study Groups

Groups	Number of animals studied radiographically	Number of animals imaged with micro PET & micro CT (imaging subgroup)	Number of animals studied histologically
Untreated control (C4 2b alone)	10	5	10
EV control (C4 2b+Empty vector)	5	5	5
RANK-Fc treatment (C4 2b+RANK-Fc)	10	5	10
RN treatment (C4 2b+RN [retronoggin])	10	5	10
RN+RANK-Fc treatment (Combined treatment group; C42b+RN+RANK-Fc)	10	5	10

Table 2

Radiological and intratibial tumor response in the study groups

Groups	Number of tibias with radiographic evidence of bone lesion	Number of tibias with histologic evidence of tumor
Untreated control	8/10*	10/10†
EV control	4/5	4/5
RANK-Fc treatment	5/9	9/9
RN treatment	5/10	8/10
RN+RANK-Fc treatment	2/9	8/9

* p=0.09 versus EV control, RANK-Fc group, RN group and RN+RANK-Fc group

† p=0.40 versus EV control, RANK-Fc group, RN group and RN+RANK-Fc group